Numerical simulation of flow field characteristics in a gas-liquid-solid agitated tank

Liangchao Li[†] and Bin Xu

Key Laboratory of Testing Technology for Manufacturing Process of Ministry of Education,
School of Manufacturing Science and Engineering, Southwest University of Science and Technology,
Mianyang, Sichuan 621010, P. R. China

Abstract−Computational fluid dynamics simulation was carried out to investigate flow field characteristics in a gas-liquid-solid agitated tank. The Eulerian multifluid model along with standard k-ε turbulence model was employed in the simulation. A multiple reference frame approach was used to treat the impeller rotation. Liquid velocity, gas holdup and solid holdup distributions in the agitated tank were obtained. The effect of operating conditions on gas and solid distributions was investigated. The predicted flow pattern was compared with results in literature. The simulation results indicate that local hydrodynamic behaviors such as velocity, gas and solid holdup distribution, are strongly influenced by operating conditions. Within the scope of our study, increasing gas inlet rate caused liquid circulation to be weakened and was not in favor of gas dispersion. Solid holdup in the upper part of the tank, especially near the wall region decreased. Adding solid loadings resulted in liquid mean velocity near the surface region decreased, gas dispersion and solid suspension becoming worse.

Keywords: Agitated Tank, Gas-liquid-solid, Three Phase Flow, Multiple Reference Frame Approach, Numerical Simulation

INTRODUCTION

Reactions involving gas, liquid and solid are widely carried out in petrochemical, wet metallurgy, environmental engineering, coal liquefaction and other industrial fields. The common multiphase reaction is gas-liquid, solid-liquid, and gas-solid system. However, some applications including three-phase system, such as gas-liquid reaction produce solid particles, and catalytic oxidation reaction. In these three phase systems, it is not the effective gas dispersion that is required, but a uniform solid suspension. To achieve these requirements, agitated tanks are widely used to carry out these reactions due to their flexibility, high efficiency and ease of control.

It is essential to understand the flow field characteristic in the three phase agitated tanks for the accurate design, scale-up and the optimization of stirred reactors. However, studies on gas-liquid-solid three phase agitated tanks are not enough, and much research is about gas-liquid [1-3] and solid-liquid [4-6] agitated tanks at present. Compared to the two-phase flow, the flow field in the gas-liquid-solid agitated tanks is more complex, and more difficult to investigate. A few researchers performed experimental studies on the gas-liquid-solid agitated tanks [7,8], but it was mainly aimed at macro parameters, such as power consumption, global gas holdup and off-bottom suspension. Few studies are about local hydrodynamic behavior, largely due to the complexity of the multiphase flow and the limitation of measurement technologies. Nevertheless, the local parameters, such as gas and solid holdup distribution and local liquid velocity, may be crucial for successful design of the agitated tank reactors.

With the development of computing technologies, computational fluid dynamics (CFD) method based on the solution of Navier-Stokes equations has become a useful and powerful tool for the prediction of flow field characteristics in agitated tanks. In comparison with the measurement methods, the CFD costs less and can be used to obtain local information which cannot be measured by experimental approaches. Two main approaches are used to model the two phase flows [9]: Eulerian-Eulerian method and Eulerian-Lagrange method. Between them, the Eulerian-Eulerian method is used by many for its timesaving and wide range of operating conditions. Kasat et al. [10] used the Eulerian-Eulerian model to study the solid suspension and liquid-phase mixing in a solid-liquid stirred reactor. Tamburini et al. [11] performed experiments and CFD simulations to analyze off-bottom suspension with Eulerian-Eulerian method in a dense solid-liquid stirred tank. Lane et al. [12] numerically modeled gas-liquid flow in aerated stirred tanks. Some have extended these models to study three-phase flow field in gas-liquid-solid agitated tanks. Murthy et al. [13] and Panneerselvam et al. [14] numerically modeled flow field in gas-liquid-solid stirred reactors, while their primary aim was to predict the critical impeller speed for solid suspension.

For better understanding the flow field characteristics, especially the local parameters in gas-liquid-solid agitated tanks, we performed numerical simulations by using the commercial package Fluent 6.2. The Eulerian multifluid model along with standard k-ε turbulence model was employed in the simulation. A multiple reference frame (MRF) approach was used to treat the impeller rotation. Our first aim was to predict flow pattern, gas and solid holdup distributions in the agitated tank, and then, the influence of operating conditions such as gas inlet rate and solid loading on flow field

†To whom correspondence should be addressed.
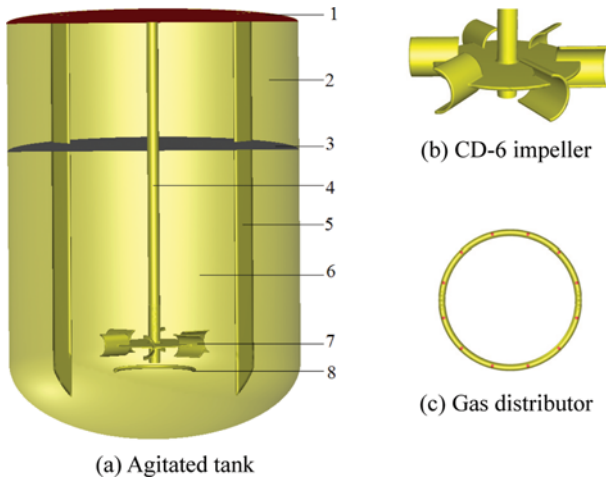E-mail: tchllc@126.com

(a) Agitated tank

(b) CD-6 impeller

(c) Gas distributor

Fig. 1. Schematic of agitated tank.

1. Gas outlet	5. Baffle
2. Air zone	6. Liquid zone
3. Liquid level	7. Impeller
4. Shaft	8. Gas distributor

characteristic.

NUMERICAL MODELS AND SIMULATION METHODS

1. Simulation Domain

The structure of the agitated tank in this study is displayed in Fig. 1, which is similar to the one in Ref. [15]. A tank of T=0.45 m in diameter with four baffles of $T/12$ and a dished base was used in the simulation. According to the symmetry of the structure and the flow field of the agitated tank, the tank is cut in half from the middle section of the two adjacent baffles, and half of them are chosen as simulation domain. The simulated media are air, sand and water at atmosphere pressure and room temperature. The properties are listed in Table 1. Air is introduced from 12 holes with the diameter of 3.0 mm on gas distributor to the agitated tank. A CD-6 impeller of 0.39T in diameter is mounted at $T/3$ height with the impeller speeds of 300 r/min being adopted for gas dispersion and solid particles suspension. The impeller speed is higher than the critical speed for solid particles off-bottom suspension. The gas inlet flow rate ranges from 5.0 to 20 m/s and the unaeration liquid level is $H=T$. To ensure the volume of liquid in the tank remained unchanged at different gas inlet rate, an air zone was set above the liquid level. Under these gas inlet rates, gas holdup in the tank is relatively low, so the breakage and coalescence of the bubbles are not considered. Bubbles are assumed to be spherical with diameter of 3.5 mm. In the same way, a mean diameter of d_s=0.1 mm for sand particles is set for the solid phase.

Table 1. Properties of simulated media at atmosphere pressure and room temperature

	Density (kg/m³)	Viscosity (Pa·s)	Diameter (mm)
Water	998	0.001003	--
Sand	2500	--	0.1
Air	1.225	1.79e-05	3.5

Fig. 2. Mesh for agitated tank.

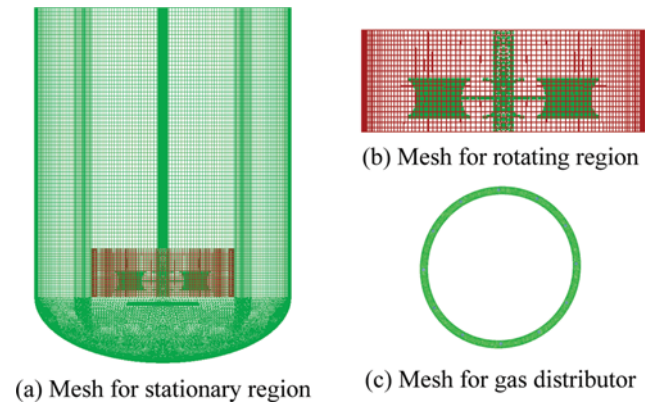(a) Mesh for stationary region

(b) Mesh for rotating region

(c) Mesh for gas distributor

2. Grid Division

A commercial grid-generation tool, Gambit 2.4 (Fluent Inc) was used to model the geometry and generate grids [16]. An MRF approach was used to treat the impeller rotation [17]. To use this approach, the agitated tank was divided into impeller rotating zone and other stationary zones, and unstructured meshes were used for the two zones as shown in Fig. 2. The impeller zone is located at $0.27 \leq h/T \leq 0.47$ and $-0.56 \leq r/R \leq 0.56$. To accurately describe the features of important surfaces, refined meshes were used on impeller blades, gas distributor and interfaces. The total elements were 619,961, which are enough for the simulation.

3. Governing Equations

The Eulerian multifluid model is used to describe the flow behavior of each phase in the agitated tank. Water is considered as continuous fluid while gas and sand of dispersed phase as pseudofluid. The mass and momentum balance equations for each phase based on the solution of Navier-Stokes equations are as follows.

Continuity equations for phase i (i=g for gas phase, l for liquid phase and s for solid phase) are given as

$$\frac{\partial}{\partial t}(\rho_i \alpha_i) + \nabla \cdot (\rho_i \alpha_i v_i) = 0 \tag{1}$$

where t is flow time, ρ is the density, α_i is holdup of phase i, and its physical meaning is the ratio of the volume of phase i to the volume for all the phases; v is the velocity vector. For the conservation of the equation, the sum of the hold up of each phase is unity, i.e.,

$$\alpha_g + \alpha_l + \alpha_s = 1.0 \tag{2}$$

The momentum balance equations for each phase have similar form and are given as,

Gas phase (dispersed fluid phase)

$$\frac{\partial}{\partial t}(\alpha_g \rho_g v_g) + \nabla \cdot (\alpha_g \rho_g v_g v_g) = -\alpha_g \nabla p$$
$$+ \nabla \cdot (\alpha_g \mu_{eff,g}(\nabla v_g + (\nabla v_g)^T)) + \alpha_l \rho_l g - F_{lg} \tag{3}$$

Liquid phase (continuous phase)

$$\frac{\partial}{\partial t}(\alpha_l \rho_l v_l) + \nabla \cdot (\alpha_l \rho_l v_l v_l) = -\varphi_l \nabla p$$
$$+ \nabla \cdot (\alpha_l \mu_{eff,l}(\nabla v_l + (\nabla v_l)^T)) + \alpha_l \rho_l g + F_{lg} + F_{ls} \tag{4}$$

Solid phase (dispersed solid phase)

$$\frac{\partial}{\partial t}(\alpha_s \rho_s v_s) + \nabla \cdot (\alpha_s \rho_s v_s v_s) = -\alpha_s \nabla p - \nabla p_s \\ + \nabla \cdot (\alpha_s \mu_{eff,s}(\nabla v_s + (\nabla v_s)^T)) + \alpha_s \rho_s g - F_{ls} \tag{5}$$

where p represents static pressure and shared by all the phases, μ_{eff} is the effective viscosity, g is gravitational force, and F is the inter-phase forces. The interphase forces include drag force, virtual mass force, lift force, wall lubrication force and the turbulence disperse force. It is reported [18] that drag force is the most important, and other forces have negligible effect on flow field characteristic in gas-liquid or solid-liquid agitated tanks. So we only considered the drag force between continuous phase and dispersed phase, and neglected other forces for simplifying the calculation.

The drag force between the liquid water and gas phase is calculated as,

$$F_{lg} = \frac{3}{4} \frac{C_{D,lg}}{d_g} \rho_l \alpha_g |v_g - v_l|(v_g - v_l) \tag{6}$$

where $C_{D,lg}$ is the drag coefficient and d_g is the bubbles diameter. In this study, the model proposed by Schiller and Naumann [19] was used to define the drag coefficient.

The drag force between the liquid water and solid phase is represented by the following equation:

$$F_{ls} = \frac{3}{4} \frac{C_{D,ls}}{d_s} \rho_l \alpha_s |v_s - v_l|(v_s - v_l) \tag{7}$$

where $C_{D,ls}$ is the drag coefficient and the model proposed by Schiller and Naumann [19] is used in present study.

The standard k-ε model for single phase flow was extended for the liquid phase turbulence in the three-phase flow system. The corresponding turbulent kinetic energy k and the turbulent energy dissipation ε are, respectively, calculated based on the following governing equation:

$$\frac{D\alpha_l \rho_l k_l}{Dt} = \nabla \left(\alpha_l \left(\mu_l + \frac{\mu_{t,l}}{\sigma_{kl}} \right) \nabla k_l \right) + \alpha_l \rho_l (P_{k,l} - \varepsilon_l) + \alpha_l \rho_l \Pi_{k,l} \tag{8}$$

$$\frac{D\alpha_l \rho_l \varepsilon_l}{Dt} = \nabla \left(\alpha_l \left(\mu_l + \frac{\mu_{t,l}}{\sigma_\varepsilon} \right) \nabla \varepsilon_l \right) + \alpha_l \frac{\varepsilon_l}{k_l} (C_{1\varepsilon} P_{k,l} - C_{2\varepsilon} \rho_L \varepsilon_l) + \alpha_l \rho_l \Pi_{\varepsilon,l} \tag{9}$$

$$\mu_{t,l} = \rho_l C_\mu \frac{k_l^2}{\varepsilon_l} \tag{10}$$

where the model constants $C_{1\varepsilon}=1.44$, $C_{2\varepsilon}=1.92$, $C_\mu=0.09$, $\sigma_k=1.0$ and $\sigma_\varepsilon=1.3$. $\Pi_{k,l}$ and $\Pi_{\varepsilon,l}$ are the influences of the dispersed phase on the continuous phase and can be obtained using the model following Elgobashi and Rizk [20].

4. Initial and Boundary Conditions

The flow field characteristic in the gas-liquid-solid agitated tank is unsteadily calculated by using Fluent 6.2 software, and the time step is 0.01 s. Although the unsteady state calculations are carried out, the final simulation results are time independent. For the initial condition, we assumed that solid particles are suspended uniformly in the liquid. Gas is introduced from gas distributor with the volume fraction of 1.0. Gauge pressure for gas outlet port is 0 Pa. As mentioned above, the simulation domain was divided into two zones to use the MRF approach, then the exchange of the mass,
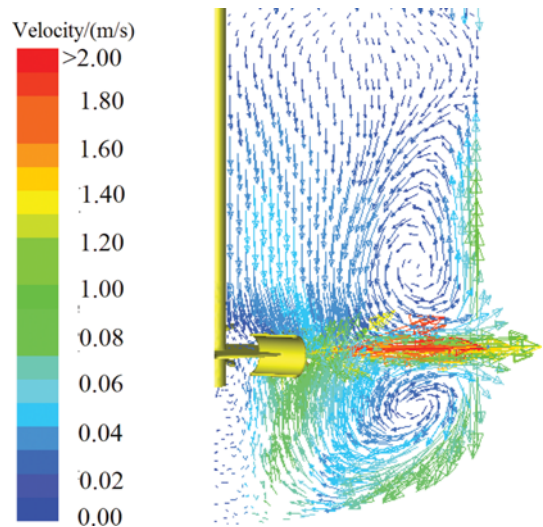

Fig. 3. Liquid velocity vector in vertical plane midway between two baffles.

momentum and energy of the two zones was achieved through the interfaces between the two zones. The tank wall, shaft, baffles and impeller surfaces are considered as nonslip boundaries for liquid phase with standard wall functions, while free slip boundaries for gas and solid phases. Based on the pressure-based implicit solver, the phase-coupled SIMPLE algorithm was employed for the pressure-velocity coupling. The first order upwind was used for the discretization of all the terms of the governing equations.

VERIFICATION OF MODELING

To verify the reliability and accuracy of our CFD simulation, the predicted flow pattern in the agitated tank and power number was compared with the results in literature.

1. Flow Pattern

Fig. 3 shows the predicted liquid velocity vector in vertical plane midway between two baffles of the tank at gas inlet rate $v_{g,in}=15$ m/s and average solid holdup $\overline{\alpha}_s=5.0\%$. It is known that the CD-6 stirrer is a radial impeller that has been studied by many researchers [15,21,22]. It can be seen from Fig. 3 that, due to the centrifugal force of the impeller rotation, liquid flow is first taken in the impeller region from the center of the impeller with upper and down direction, and then discharged from the tip of the blades in radial direction to the near wall region where liquid flow splits into two streams with each stream forming a circulation loop below and above the CD-6 stirrer. Then, the typical double circulation flow pattern is formed in the agitated tank as shown in Fig. 3. Double circulation flow pattern is commonly generated by the radial impeller. The simulated results are consistent with the flow pattern generated by radial impeller in literature [23,24], which verifies the correctness of our numerical simulations.

2. Power Number

The parameter of impeller power number N_p is commonly used to verify the CFD simulation, which reflects the accuracy of simulated flow field in the agitated tank as a whole. Up to now, the impeller power number for multiphase system has been hard to deter-

mine for the inhomogeneity of density distribution in the agitated tank. To overcome the effect of density changes, in the present work, the power number is determined under the operating condition of unaeration and zero solid loading. Then, the power number can be calculated as follows:

$$P = 2\pi T_0 N \tag{11}$$

$$N_P = \frac{P}{\rho_l N^3 D^5} \tag{12}$$

where T_0 is the impeller torque and can be obtained from the CFD simulation results directly; ρ_l is liquid density, N is impeller speed and D is impeller diameter.

The impeller power number is closely related to the geometrical parameters of the agitated tank, such as the structure of the tank, impeller to tank diameter ratio and clearance of the impeller from the tank bottom. Table 2 gives the comparison of CD-6 stirrer power number of present work with data in literature [22,25] for the impeller mounted at T/3 height from the bottom of tank. To better compare with the data in literature, the structure of the tank in the present work 2 is consistent with that in literature. It can be seen that the power number of present work 1 is smaller than that of present work 2. The reason may be is the dished base for the agitated tank of present work 1. On the whole, the simulated power numbers are close to the data in literature, which verifies the accuracy of CFD simulation in present work.

Table 2. Comparison of power number predicted by this work with data in literature

Literature	Geometry	Np
Present work 1	T=H=0.45 m, D=0.39T, dished base	2.66
Present work 2	T=H=0.476 m, D=0.4T, flat base	3.19
Ref. [25]	T=H=0.476 m, D=0.4T, flat base	3.10
Ref. [22]	T=H=0.476 m, D=0.4T, flat base	3.08

RESULTS AND DISCUSSION

1. Gas Dispersion and Solid Suspension in the Agitated Tank
1-1. Gas Holdup Distribution

Gas holdup is a key parameter for gas dispersion in gas-liquid and gas-liquid-solid agitated tanks, and has been extensively studied by researchers. An understanding of the gas holdup distribution would significantly facilitate the design of agitated tanks.

The contours of gas holdup in different planes in the tank are shown in Fig. 4. For the buoyancy of air bubbles, gas moves up mainly after discharge from the tip of the blades, and gas holdup in bottom region is almost zero. Gas holdup near the center of the upper circular vortex is relatively high. It is mainly caused by the relative relationship between liquid velocity and gas rise up velocity, and ineffective gas dispersion there. Gas holdup behind the blades is very high. It can be interpreted that pressure behind the blades is very low and the gas is easy to accumulate there to form the so-called gas cavity. The gas cavity behind the blade would decrease the impeller capacity and is not favorable for gas dispersion. Gas holdup behind the baffles is also relatively high for the stagnate zone there.

1-2. Solid Holdup Distribution

Fig. 5 shows solid holdup distribution in different planes. On the whole, the solid holdup decreases with height from bottom to liquid surface. The highest solid holdup is found in the center of bottom region. Also, the solid holdup in the center of circulation vortex is relatively low, which is due to centrifugal force there. As we know, sand density is larger than air and water density. Thus, under centrifugal force caused by circular vortex, low density media are easier to gather in the center of the vorticity, leading to the low solid holdup there, which is somewhat similar to the operating principle of solid-liquid cyclone.

2. Effect of Gas Inlet Rate on Flow Field
2-1. Effect of Gas Inlet Rate on Liquid Velocity

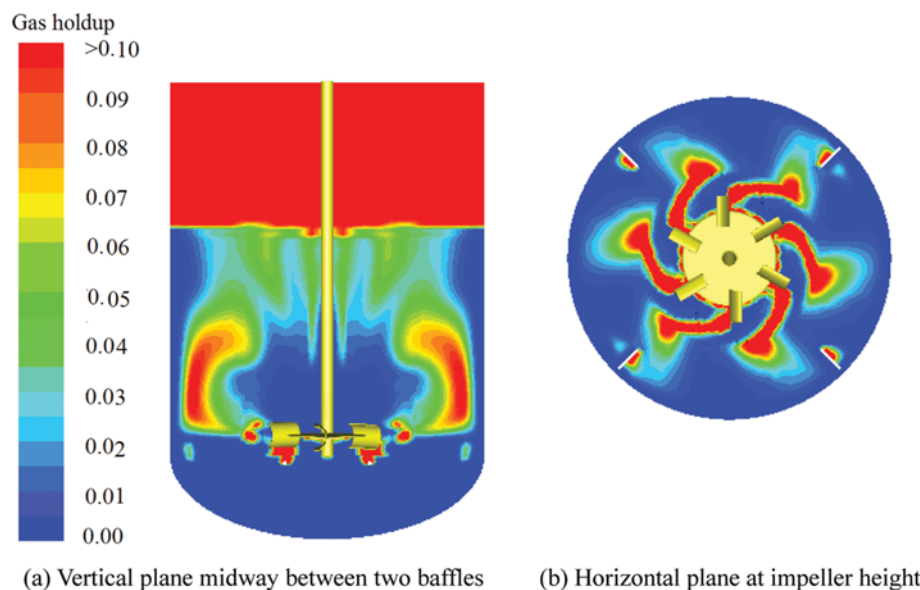Fig. 6 shows the effect of gas inlet rate on liquid velocity distri-

(a) Vertical plane midway between two baffles   (b) Horizontal plane at impeller height

Fig. 4. Gas holdup distribution in different planes ($v_{g,in}$=15 m/s, $\bar{\alpha}_s$=5.0%)

(a) Vertical plane midway between two baffles   (b) Horizontal plane at impeller height
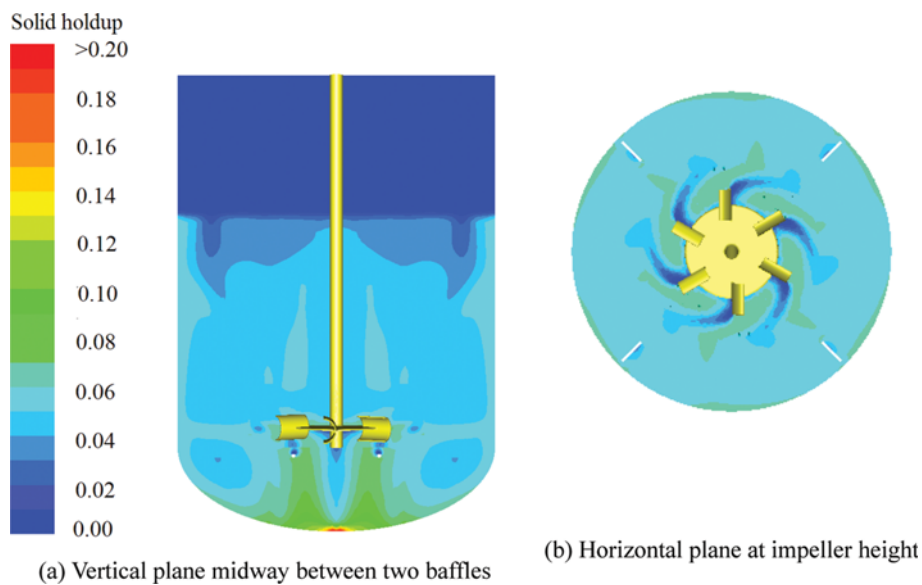
Fig. 5. Solid holdup distribution in different planes ($v_{g, in}$=15 m/s, $\overline{\alpha}_s$=5.0%).
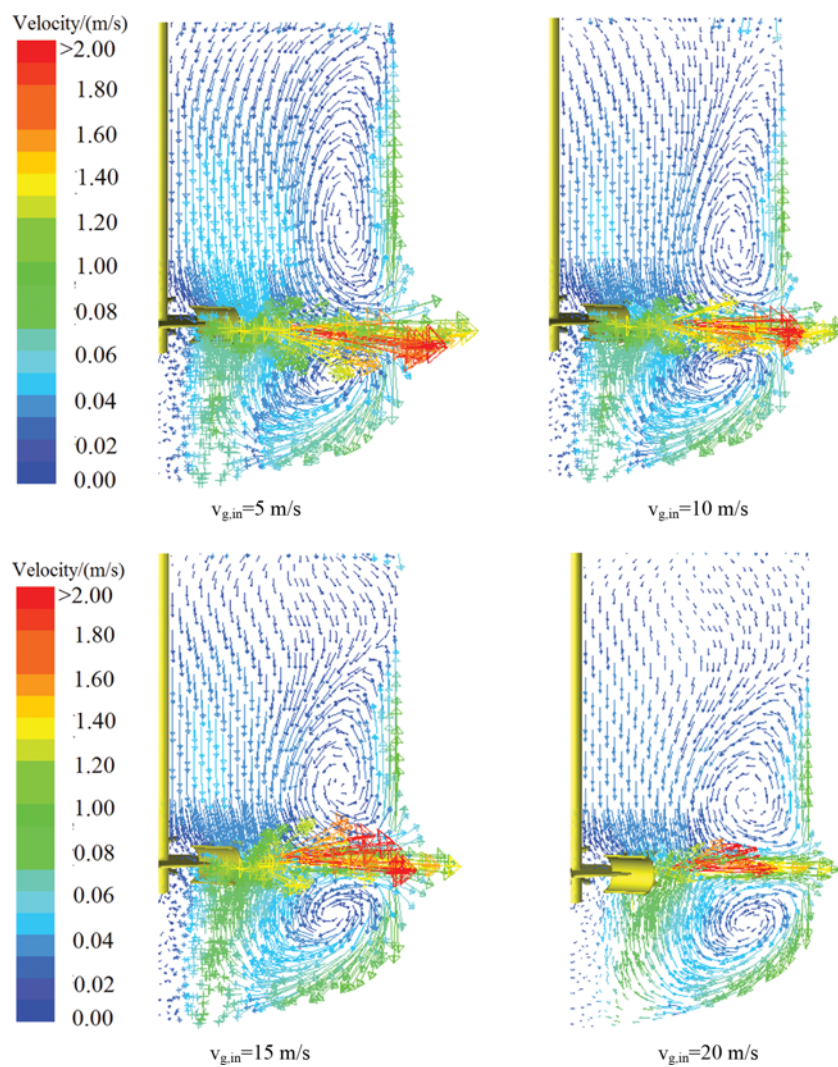
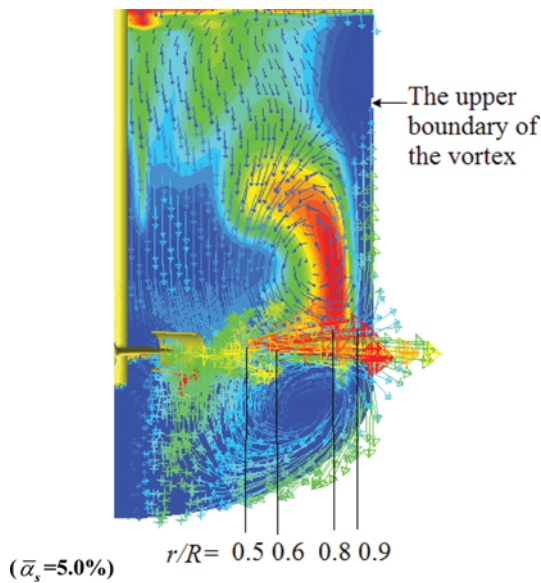**Fig. 6. Liquid velocity vectors in vertical plane for different gas inlet rates ($\overline{\alpha}_s$=5.0%).**

$(\overline{\alpha}_s = 5.0\%)$

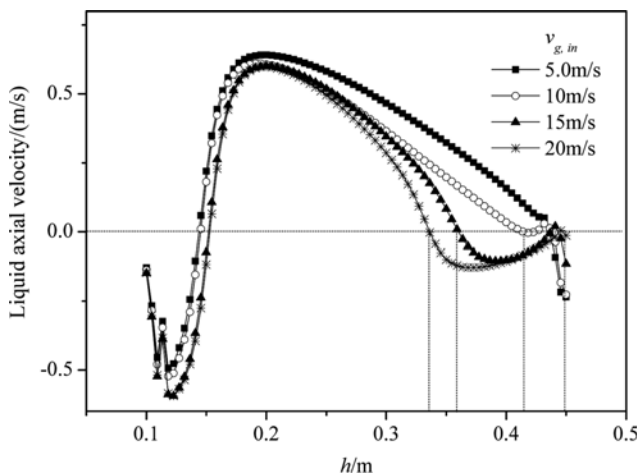**Fig. 7. The overlay graph of liquid velocity vectors and gas holdup distribution in vertical plane.**

Fig. 8. Liquid axial velocity distribution at different gas inlet rates (r/R=0.9, $\overline{\alpha}_s$=5.0%).

bution in the agitated tank. From the figure we can see that, on the whole, the liquid velocity decreases and the circulation vortex decreases with the increase of gas inlet rates. Fig. 7 gives an overlay graph of liquid velocity vectors and gas holdup distribution in a vertical plane midway between two baffles. It can be seen that the location of vortex upper boundary can be determined where the liquid axial velocity is zero. Fig. 8 gives the axial velocity distributions at radial location of r/R=0.9 with different gas inlet rates. The height of vortex upper boundary decreases from 0.45 m to 0.34 m when the gas inlet rate rises from 5 to 20 m/s. The simulation results indicate that the increasing of gas inlet rate causes liquid circulation to be weakened. Similar results about the effect of aeration on liquid mean velocity in a tank stirred by a down-and up-pumping axial flow impeller were reported by Aubin [26].

Fig. 9 gives a quantitative analysis of liquid mean velocity axial distribution with different gas inlet rates at three radial locations. It
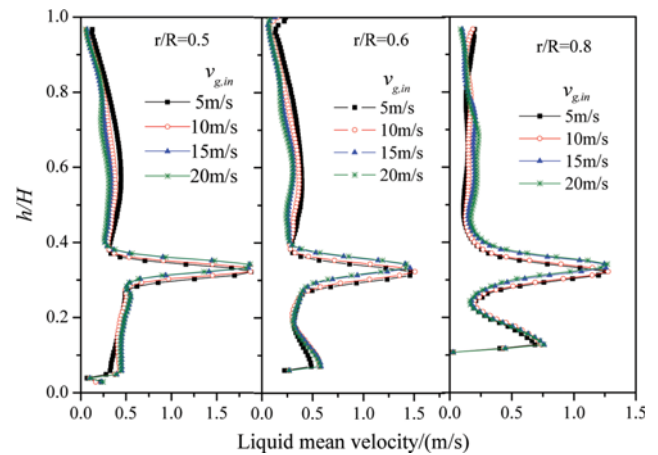

Fig. 9. Axial distribution of liquid mean velocity for different gas inlet rates at three radial locations ($\overline{\alpha}_s$=5.0%).

is observed that the effect of gas inlet rates on liquid mean velocity varies with regions. For the impeller region, the liquid velocity is significantly impacted by the high speed of blades and has a velocity peak at impeller mounting height. The mean velocity peak moves up slightly at large gas inlet rate for the effect of gas buoyancy. From upper circulation vortex to liquid surface regions, the effect of the gas inlet rates on liquid mean velocity varies with radial locations. From Fig. 7 we can see that the downward direction of liquid axial velocity is opposite to that of gas rise up velocity at radial locations of r/R=0.5 and 0.6. So the rising gas has a weakening effect on liquid mean velocity at these two radial locations as shown in Fig. 9. For the radial location of r/R=0.8, the direction of the liquid velocity is the same as that of gas rise up velocity (see Fig. 7) at axial height of 0.33<h/H<0.8; rising gas plays an accelerating effect on the liquid velocity. At axial height of h/H>0.8, the direction of gas rise up velocity is opposite to that of liquid velocity, and rising gas weakens the mean liquid velocity again. In addition, liquid mean velocity increases with increasing of gas inlet rates in bottom region, especially in radial locations of r/R=0.5 and 0.6. It may be the aeration causes the liquid velocity rise in the bottom region.

2-2. Effect of Gas Inlet Rate on Gas Holdup Distribution

The gas inlet rate greatly influences the gas holdup distribution in agitated tanks. Figs. 10 and 11 show gas holdup distribution in the agitated tank with different gas inlet rates. With increasing of the gas inlet rate, gas holdup rises in most regions of the tank. Gas holdup distribution is closely related to liquid circulation vortex. As shown in Fig. 7, gas is discharged from the tip of blades along with liquid. First, the direction of gas rise up velocity is the same as that of liquid velocity, and then, in the upper part of the liquid circulation vortex, liquid flows gradually from wall region to the center of the tank, which drives bubbles together to the center of the tank. Finally, gas escapes from the center of the liquid surface. In the upper part of the liquid circulation vortex, the rising bubbles are hindered by the liquid flow for the opposite direction of liquid axial velocity to gas rise up velocity. Therefore, gas accumulates easily in the rising channel and forms high local gas holdup at a height of 0.33<h/H<0.8, as shown in Fig. 11. At the same time, bubbles disperse gradually in the rising process in the liquid. In fact,

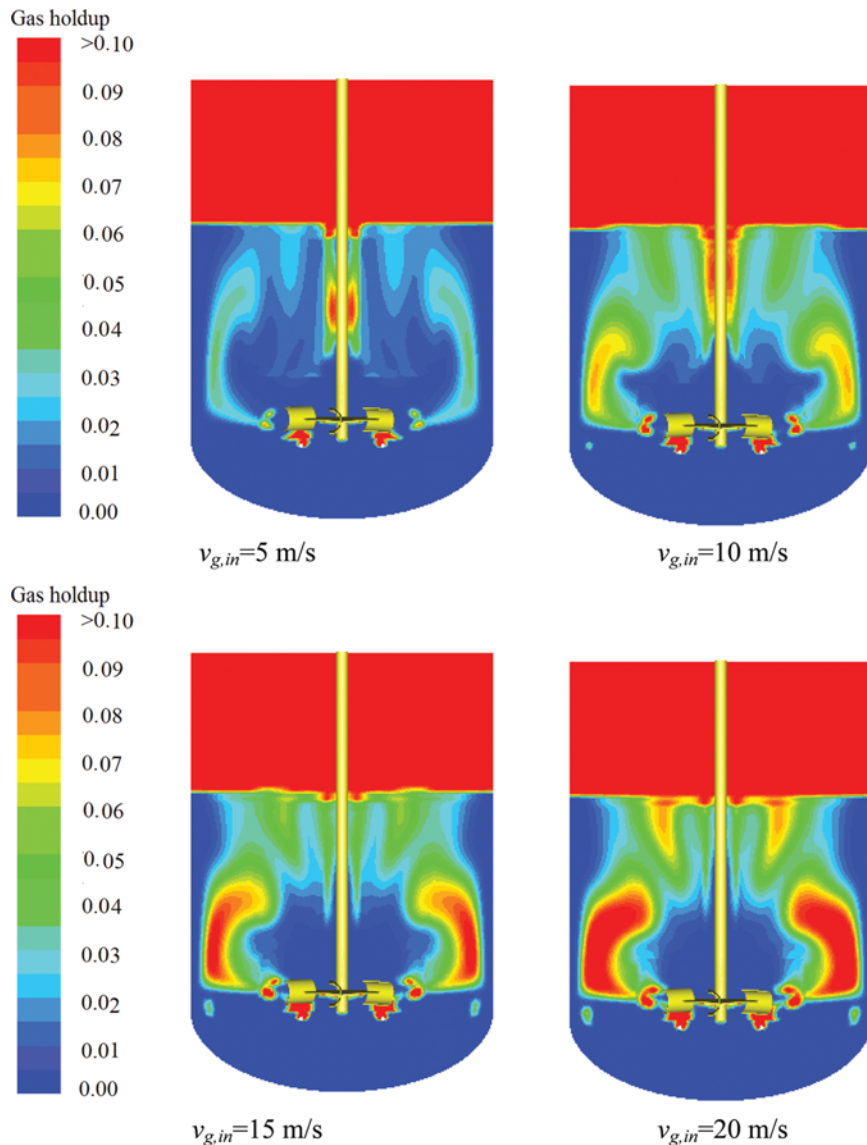Fig. 10. Gas holdup distribution in planes for different gas inlet rates ($\overline{\alpha}_s$=5.0%).
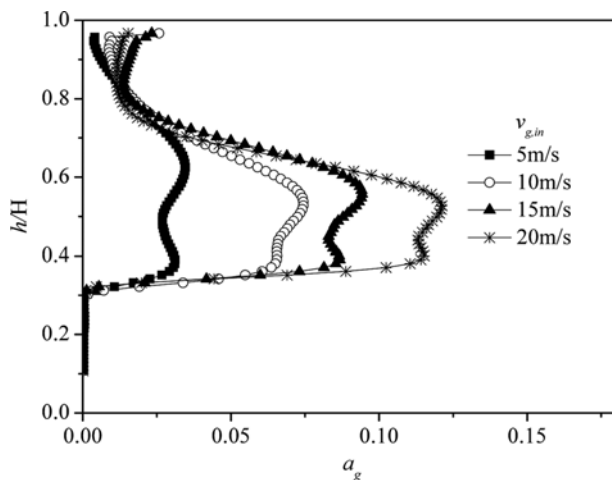

Fig. 11. Effect of gas inlet rates on axial gas holdup distribution ($\overline{\alpha}_s$= 5.0%, r/R=0.8).

the uniformity of gas holdup distribution becomes worse at larger gas inlet rates. The simulated results indicate that increasing the gas inlet rate can improve the global gas holdup in the agitated tank, while its distribution uniformity becomes worse.

2-3. Effect of Gas Inlet Rate on Solid Holdup Distribution

The effect of gas inlet rate on solid holdup distribution is very complex. It mainly includes the following three aspects. First, large gas inlet rates cause the impeller mixing ability to be reduced and liquid mean velocity decreases in many regions, as discussed previously. The results will cause that the impeller cannot provide enough energy to make solid particles being suspended. Second, the rise of the gas plays a role in suspension of solid particles. Third, with increasing of gas inlet rate, the fluid space becomes larger, which will dilute the particle concentration. The solid suspension becomes better or worse, depending on which factors have a greater impact. Fig. 12 gives solid holdup distribution in a vertical plane with gas inlet rate varying from 5 to 20 m/s. It can be seen that, with increas-
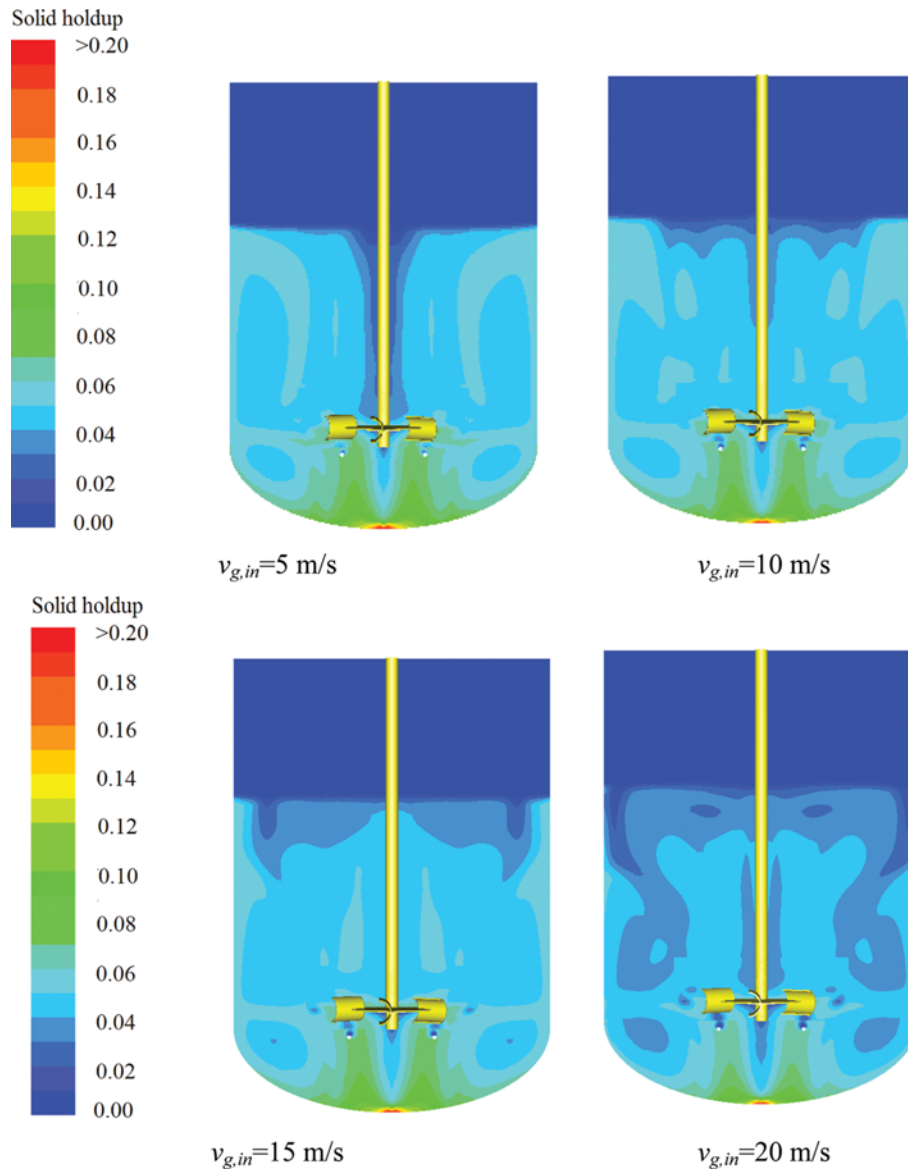
Fig. 12. Solid holdup distribution in vertical plane for different gas inlet rates ($\overline{\alpha}_s$=5.0%).

ing of gas inlet rates, solid holdup distribution in the agitated tank changes greatly. On the whole, particle concentration in the upper part of the tank becomes dilute at larger gas inlet rate, especially near the wall region. In the center region of the liquid surface, solid holdup decreases slowly with increasing of gas inlet rates. It is mainly due to a large number of bubbles escaping from the center of the liquid surface. The rising gas can make particles be suspended there.

Fig. 13 gives the axial solid holdup distribution at radial location of r/R=0.9 with different gas inlet rates. Solid holdup reaches the highest value in the upper part of the tank and then decreases gradually. The location of highest solid holdup can be considered as that most of the particles can be suspended there. As shown in Fig. 13, the location of highest solid holdup decreases from 0.42 m to 0.31 m when the gas inlet rate rises from 5 to 20 m/s. It demonstrates that solid suspension becomes worse at larger gas inlet rate at the radial location.
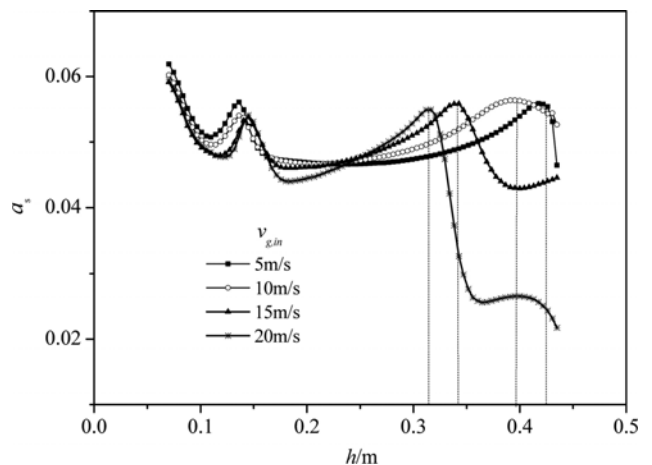

Fig. 13. Effect of gas inlet rates on axial solid holdup distribution ($\overline{\alpha}_s$=5.0%, r/R=0.9).
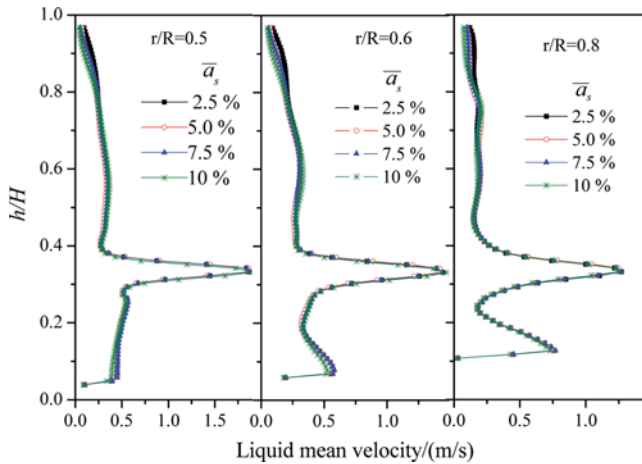
Fig. 14. Effect of solid loading on liquid mean velocity axial distribution ($v_{g,in}$=15 m/s).

Fig. 16. Radial gas holdup distribution with different solid loadings ($v_{g,in}$=15 m/s, h/H=0.9).

3. Effect of Solid Loading on Flow Field

3-1. Effect of Solid Loading on Liquid Velocity

Fig. 14 gives axial distributions liquid mean velocity with different solid loadings at three radial locations. The liquid mean velocity in most of the regions changes slightly with the average solid holdup varying from 2.5 to 10%. Liquid mean velocity decreases near the surface region with increasing of solid loading. Geisler [27] and Kasat [10] also obtained that particles lead to the liquid mean velocity being reduced near the top surface in solid-liquid stirred reactors. In addition, Montante [4] PIV measured the liquid mean velocity near the impeller region in a dilute solid-liquid stirred tank and found the effect of solids on mean velocity was negligible. Overall, the CFD simulation result in the present work is in agreement with that in literature [4,10,27]. The low solid loadings and small particles size may be the main reasons for the little impacts on liquid mean velocity in most regions. As for the near surface region, since it is far from the impeller, the hindering effect of solid
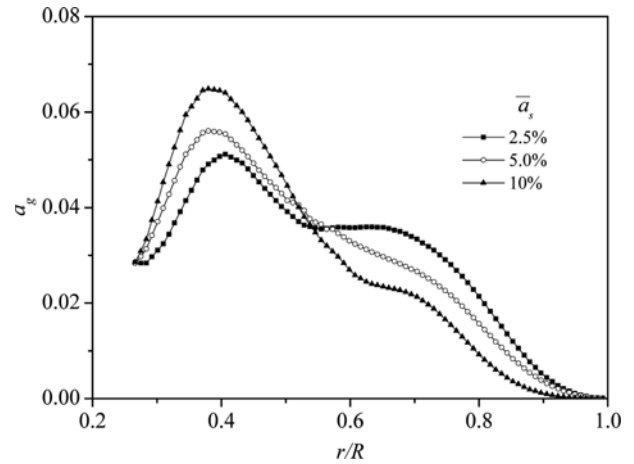
particles on liquid velocity increases.

3-2. Effect of Solid Loading on Gas Holdup Distribution

Fig. 15 shows the gas holdup distribution in vertical planes with two different solid loadings. From the color change of contour map we can see visually that gas holdup in the agitated tank decreases slightly when the average solid holdup rises from 5.0 to 10%. Fig. 16 gives the radial gas holdup distribution near the liquid surface. With increasing of solid loadings, gas holdup in the center of the liquid surface increases, while decreases near the wall region. It shows that gas more easily escapes from the center of the liquid surface and cannot be effectively dispersed for higher solid loadings. The simulation results indicate that gas dispersion becomes worse with increasing solid loadings in the agitated tank.

3-3. Effect of Solid Loading on Solid Holdup Distribution

Fig. 17 shows the axial solid holdup distribution for different solid loadings. The axial solid holdup distribution is very uniform for low solid loading. With increasing of solid loadings, solid holdup
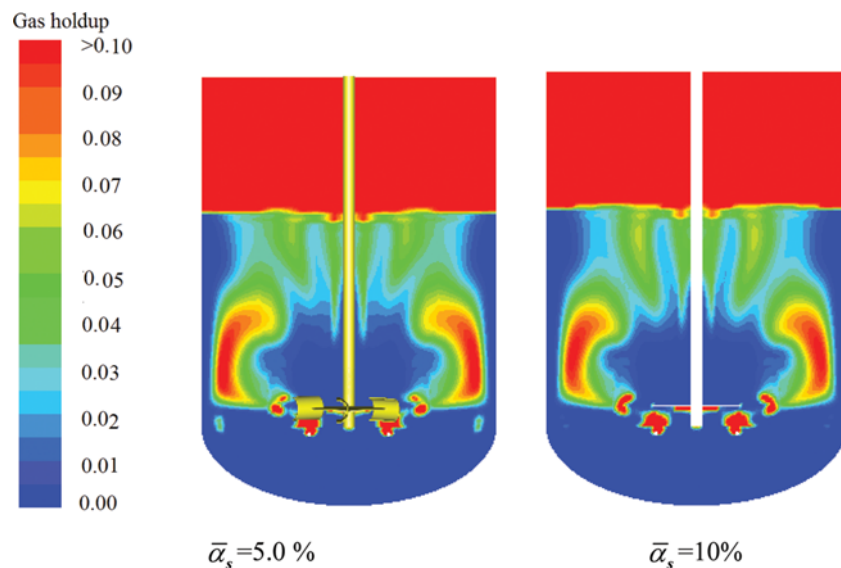

Fig. 15. Gas holdup distribution in vertical planes for different solid loadings ($v_{g,in}$=15 m/s).
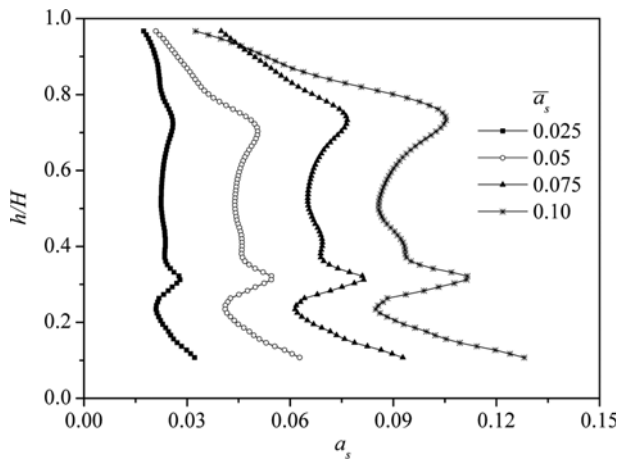
Fig. 17. Axial solid holdup distribution for different solid loadings ($v_{g, in}$=15 m/s, r/R=0.8).

in the upper part of the tank becomes relatively lower, and more particles easily gather in the bottom regions of the tank. The simulation results demonstrate that adding solid loadings worsens solid suspension. It may be the reason that the liquid mean velocity decreases in the upper part of the tank for higher solid loadings, as discussed previously, which leads to low solid holdup there.

CONCLUSIONS

(1) Numerical simulations of flow field characteristic in a gas-liquid-solid stirred tank employed the Eulerian multi-fluid approach along with the standard k-ε turbulence model. The typical double circulation flow pattern and power number generated by a CD-6 impeller were predicted, which agree with that in literature. In general, the numerical simulations are capable of predicting the flow field in the agitated tank under different operating conditions.

(2) Increasing gas inlet rate causes liquid circulation to be weakened. The effect of gas inlet rates on liquid mean velocity varies with regions. At larger gas inlet rates, the global gas holdup rises while gas holdup distribution uniformity becomes worse, and particle concentration in the upper part of the tank becomes dilute, especially near the wall region.

(3) Solid loading influences the flow field characteristic in the gas-liquid-solid stirred tank. On the whole, with increasing solid loading, liquid mean velocity near the liquid surface region decreases, and gas dispersion and solid suspension become worse.

ACKNOWLEDGEMENTS

NOMENCLATURE

C_1, C_2, C_μ : turbulence model constants [-]
C_D : drag coefficient [-]
d : diameter of the dispersed phase particles [m]
D : impeller diameter [m]
F : interphase forces [N/m^3]
g : gravitational force [m/s^2]
h : axial location in the tank [m]
H : height of unaeration liquid [m]
k : turbulent kinetic energy [m^2/s^2]
N : impeller speed [1/s]
Np : power number [-]
p : static pressure [Pa]
P : power consumption [W]
r : radial location in the tank [m]
R : radius of the tank [m]
t : time [s]
T : diameter of the tank [m]
T_0 : impeller torque [N m]
v : velocity vector [m/s]

Greek Letters

α : phase holdup
ε : turbulent energy dissipation [m^2/s^3]
μ_{eff} : effective viscosity [kg/m s]
ρ : density [kg/m^3]
σ_k, σ_ε : turbulent model constants [-]

Superscripts

$-$: average

Subscripts

i : number of phases
g : gas phase
l : liquid phase
s : solid phase

REFERENCES

1. M. Petitti, A. Nasuti, D. L. Marchisio, M. Vanni, G. Baldi, N. Mancini and F. Podenzani, *AIChE J.*, **56**, 36 (2010).
2. M. Bouaifi, G. Hebrard, D. Bastoul and M. Roustan, *Chem. Eng. Process.*, **40**, 97 (2001).
3. S. S. Alves, C. J. Maid, J. M. T. Vasconcelos and A. J. Serralheiro, *Chem. Eng. J.*, **89**, 109 (2002).
4. G. Montante, M. H. Occulti and F. Magelli, *PIV Measurements of Mean Flow and Turbulence Modulation in Dilute Solid Liquid Stirred Tanks*, 15th Int Symp on Applications of Laser Techniques to Fluid mechanics Lisbon Portugal, July 5-8 (2010).
5. R. Angst and M. Kraume, *Chem. Eng. Sci.*, **61**, 2864 (2006).
6. R. N. Sharma and A. A. Shaikh, *Chem. Eng. Sci.*, **58**, 2123 (2003).
7. Y. Y. Bao, Z. G. Hao, Z. M. Gao, L. T. Shi and J. M. Smith, *Chem. Eng. Sci.*, **60**, 2283 (2005).
8. N. Dohi, Y. Matsuda, K. Shimizu, K. Minekawa and Y. Kawase, *Chem. Eng. Process.*, **41**, 267 (2002).
9. J. J. Derksen, *AIChE J.*, **49**, 2700 (2003).
10. G. R. Kasat, A. R. Khopkar, V. V. Ranade and A. B. Pandit, *Chem. Eng. Sci.*, **63**, 3877 (2008).
11. A. Tamburini, A. Cipollina, G. Micale, M. Ciofalo and A. Brucato, *Chem. Eng. Res. Design*, **87**, 587 (2009).

12. G. L. Lane, M. P. Schwarz and G. M. Evans, *Appl. Mathematical Modeling*, **26**, 223 (2002).

13. B. N. Murthy, R. S. Ghadge and J. B. Joshi, *Chem. Eng. Sci.*, **62**, 7184 (2007).

14. R. Panneerselvam, S. Savithri and G. D. Surender, *Chem. Eng. Res. Design*, **86**, 1331 (2008).

15. Z. M. Gao, J. M. Smith and H. Müller-Steinhagen, *Chem. Eng. Process.*, **40**, 489 (2001).

16. Fluent Inc., Gambit Modeling Guide. Lebanon: Fluent Inc., 41 (2006).

17. Fluent Inc., User's Manual to FLUENT 6.1. Fluent Inc. Centrera Resource Park, 10 Cavendish Court, Lebanon, USA (2004).

18. R. Panneerselvam, S. Savithri and G. D. Surender, *Ind. Eng. Chem. Res.*, **48**, 1608 (2009).

19. L. Schiller and Z. Naumann, *Z. Ver. Deutsch. Ing.*, **77**, 318 (1935).

20. S. E. Elgobashi and M. A. Rizk, *Int. J. Multiphase Flow*, **15**, 119 (1989).

21. A. M. Lupasteanu, A. I. Galaction and D. Cascaval, *Romanian Society of Biological Sciences*, **13**, 3821 (2008).

22. N. N. Qi, G. Y. Wu, H. Wang, K. Zhang and H. Zhang, *J. Chem. Industry Eng. (China)*, **61**, 2305 (2010).

23. D. Wadnerkar, R. Utikar, M. O. Tade and V. K. Pareer, *Adv. Power Technol.*, **23**, 445 (2012).

24. N. N. Qi, H. Zhang, K. Zhang, G. Xu and Y. P. Yang, *Particuology*, **11**, 317 (2013).

25. Z. Li, *Experimental investigation and numerical simulation of flow characteristics in vessels stirred by disc turbines*, Beijing: Beijing University of Chemical Technology (2007).

26. J. Aubin, N. Le Sauze, J. Bertrand, D. F. Fletcher and C. Xuerer, *Experimental Thermal Fluid Sci.*, **28**, 447 (2004).

27. R. K. Geisler and A. B. Mersmann, *Local velocity distribution and power dissipation rate of suspension in stirred vessels*, 6th European Conference on Mixing, Pavia, Italy, 267 (1988).